Korean J. Chem. Eng., **26**(2), 332-338 (2009)

The spatiotemporal instability on mixed convection in porous media

Tae Joon Chung*,†, Min Chan Kim, and Chang Kyun Choi*****

*R&D center, Samsung Electro-Mechanics, Suwon 443-370, Korea
**Department of Chemical Engineering, Jeju National University, Jeju 690-756, Korea
***School of Chemical and Biological Engineering, Seoul National University, Seoul 151-744, Korea
(*Received 7 May 2008 • accepted 3 September 2008*)

Abstract−The absolute and convective instability on mixed convection in porous media is examined, and the phase transition from the oscillatory wave motion to the stationary vortex one is observed. Based on linear and weakly nonlinear analyses, the critical conditions to mark the onset of traveling transverse rolls are analytically obtained for small Péclet numbers. The flow change from transverse wave to longitudinal vortex is reproduced by numerical simulation. These criteria made good agreement with the available experiment data.

Key words: Absolute Instability, Convective Instability, Porous Media

INTRODUCTION

It is well known that natural convection can occur when a fluid-saturated porous medium such as the ground water and the packed bed reactor is heated from below [1,2]. The convection in porous media is important from the viewpoint of both science and engineering, e.g., mantle recurrence, oil recovery and storage of grain. A large number of theoretical and experimental studies have been reported on this Horton-Rogers-Lapwood convection. However, overall in an actual system, the instability phenomena through the porous media are very much complicated due to a certain external forces, such as inertial, electrical field or magnetic force. When the inertial force exists owing to a flow of fluid, the spatiotemporal motion appears at a critical condition because of the competition between inertial and buoyancy forces.

Prats [3] showed that in the porous media heated from below the horizontal throughflow would bring time-dependent oscillations in temperature and velocity fields. Combarnous and Bia [4] observed experimentally that with increasing the flow rate a flow change occurs from traveling transverse rolls to stationary longitudinal ones. In a horizontal porous layer with through flow Hsu and Cheng [5] analyzed the critical position marking the onset of vortex instability. Choi and his colleague studied stationary vortex instability in a fluid and fluid-saturated porous layer with propagation theory and experiment [6-8]. Lee et al. [9] expected the onset of mixed convection in an inclined surface embedded porous media heated from below with propagation theory. His prediction had good agreement with experiment data using an electrochemical deposition system. Chung et al. [10] extended the instability limit from Darcy region to Forchheimer one on a horizontal porous system heated isothermally from below. For a constant heat flux system, Park et al. [7] predicted the onset of stationary vortex instability with numerical simulation. According to their results the critical distance predicted by the propagation theory marked the intrinsic instability, and the magnification of mixed convection appeared after growth of an infinitesimal instability through thermal boundary layer thickness. Recently, Combarnous and coworkers [4,11,12] analyzed the spatiotemporal instability of mixed convection flow in porous media heated from below and compared with experiment. They showed a lower boundary of instability. However, on the transition from the oscillatory wave rolls in the upstream to the stationary vortex ones in the downstream, its detailed mechanism and overview of stability condition are still ambiguous.

In the present study, we focused on spatiotemporal convective motion in the horizontal porous layer heated isothermally from below. The lower bound of stability is obtained with a linear stability analysis. In connection with the qualitative transition from an absolute instability to a convective one, the Ginzburg-Landau equation (GLE) was developed with weakly nonlinear analysis. Furthermore, in order to observe the flow transition from the oscillatory transverse rolls to the stationary ones, we adopted the direct 3-dimensional simulation considering control volume. The stability diagram derived from these analyses was compared with the available analysis and experiment [4,11-13].

THEORETICAL ANALYSIS

1. Governing Equations

The system considered here is the fluid-saturated porous media confined between two horizontal rigid boundaries. There exists a uniform superficial velocity U_0 in the X-direction through the porous medium. The fixed upper boundary temperature T_i is smaller than the lower one $T_w(>T_i)$. Under forced convection the temperature profile is vertically linear. The characteristic outline is shown in Fig. 1.

With small U_0 but large $\Delta T(=(T_w-T_i)$, buoyancy-driven convection can set in. Under very weak mixed convection, the important parameters to control the present system are the Darcy-Rayleigh number R and the Péclet number Pe:

$$R=\frac{g\beta\Delta TKH}{\alpha\nu},\quad Pe=\frac{U_0H}{\alpha}, \tag{1a-b}$$

†To whom correspondence should be addressed.
E-mail: camus1@snu.ac.kr
‡This paper is dedicated to Professor Chang Kyun Choi to celebrate his retirement from the school of chemical and biological engineering of Seoul National University.

where g, H, K, α, β and ν denote the gravitational acceleration, the vertical depth of the porous layer, the permeability, the thermal diffusivity, the thermal expansivity, and the kinematic viscosity, respectively. For homogeneous porous materials the dimensionless governing equations are given under the Darcy law, Boussinesq approximation and local thermal equilibrium as usual:

$$\nabla\cdot\mathbf{u}=0, \tag{2}$$

$$\mathbf{u}=-\nabla p+R\theta\mathbf{k}, \tag{3}$$

$$\frac{\partial\theta}{\partial\tau}+\mathbf{u}\cdot\nabla\theta=\nabla^2\theta, \tag{4}$$

where $\mathbf{u}$, p, θ, τ and $\mathbf{k}$ denote the velocity vector (=u$\mathbf{i}$+v$\mathbf{j}$+w$\mathbf{k}$), pressure, temperature, time and the vertical unit vector, respectively. The operator ∇^2 is the Laplacian. The velocity, temperature, pressure, time, and distance have the scale of α/H, ΔT, $\rho\alpha\nu$/K, H^2/α, and H, respectively. Here ρ represents the density of fluid. Under the basic state of Darcy flow, it is noted that u=Pe but v=w=0.

2. Linear Stability Analysis

To examine the stability condition to mark a convective motion, a linear stability analysis is employed. Therefore, the physical quantities such as the temperature and the velocity are linearized as sum of the basic condition and the infinitesimal perturbed one in Eqs. (2)-(4), i.e., $\langle\bullet\rangle=\langle\bullet\rangle_b+\langle\bullet\rangle'$, where the bracket, $\langle\bullet\rangle$ means the physical quantities, the subscript 'b' the basic condition and the superscript '′' the perturbed one. The vertically linear temperature is considered as the basic condition when a fluid-flow is absent. In addition, for the periodic disturbances the following form of disturbance under normal mode analysis is introduced into the linearized equations:

$$(\theta',\mathbf{u}')=(\hat{\theta}(z),\hat{\mathbf{u}}(z))\exp[i(a_x x+a_y y)+\sigma\tau], \tag{5}$$

where i denotes the imaginary number ($=\sqrt{-1}$), and a_x as well as a_y the wavenumbers in the horizontal directions. The time-evolution term σ consists of the real part and imaginary one ($=\sigma_r+i\sigma_i$). The real part σ_r represents the temporal growth rate, and the imaginary one σ_i the frequency or the dispersion related to an oscillating mode. The functions $\hat{\theta}$ and $\hat{\mathbf{u}}$ satisfy the vertical boundary conditions. Using Eqs. (2)-(5) under σ_i=0, the growth rate is obtained as a function of the horizontal wavenumber $a(=\sqrt{a_x^2+a_y^2})$:

$$\sigma_r=(n^2\pi^2+a^2)\left[\frac{R}{(n^2\pi^2+a^2)^2/a^2}-1\right]. \tag{6}$$

For σ_r=0 and n=1 the minimum bound of R is derived. This neutral stability curve yields the well-known critical conditions to mark the onset of buoyancy-driven convection in form of stationary waves, $R_{c,0}$ and $a_{c,0}$:

$$R_{c,0}=4\pi^2,\ a_{c,0}=\pi. \tag{7a-b}$$

For $R<R_{c,0}$ the system is stable.

Here, we consider the weak throughflow along the x-direction. For the traveling transverse rolls Eq. (5) can be changed to the following periodic disturbances at $R=R_{c,0}$:

$$\begin{pmatrix} w_1(x,z,\tau)\\ \theta_1(x,z,\tau)\end{pmatrix}=\begin{pmatrix}\hat{w}(z)\\ \hat{\theta}(z)\end{pmatrix}\exp\{i(a_c x-\omega_c\tau)\}+\text{c.c.}, \tag{8}$$

where 'c.c.' denotes the corresponding complex conjugates and ω_c is the imaginary part of $\sigma(=\sigma_i)$. Substituting Eqs. (8) into (2)-(4), the stability equations are produced:

$$\begin{bmatrix}(D^2-a_c^2) & a_c^2R_c\\ 1 & i\omega_c+(D^2-a_c^2)-ia_cPe\end{bmatrix}\begin{bmatrix}\hat{w}(z)\\ \hat{\theta}(z)\end{bmatrix}=0, \tag{9a}$$

$$\hat{w}=D\hat{w}=\hat{\theta}=0 \quad \text{at} \quad z=0 \quad \text{and} \quad z=1, \tag{9b}$$

where D=d(·)/dz.

For small Pe, the solution of Eqs. (9) is obtained near the critical condition by following the procedure of Müller et al. [4]. The variables are expanded with respect to small Pe:

$$\begin{pmatrix}\hat{w}(z)\\ \hat{\theta}(z)\end{pmatrix}=\begin{pmatrix}\hat{w}_0(z)\\ \hat{\theta}_0(z)\end{pmatrix}+i\begin{pmatrix}\hat{w}_1(z)\\ \hat{\theta}_1(z)\end{pmatrix}Pe+\begin{pmatrix}\hat{w}_2(z)\\ \hat{\theta}_2(z)\end{pmatrix}Pe^2+O(Pe^3), \tag{10a}$$

$$R_c=R_{c,0}+R_{c,2}Pe^2+O(Pe^4), \tag{10b}$$

$$a_c=a_{c,0}+a_{c,2}Pe^2+O(Pe^4), \tag{10c}$$

$$\omega_c=\omega_{c,1}Pe+O(Pe^3). \tag{10d}$$

Here, it is noted that R_c has been expanded with even orders of Pe due to the symmetry, but ω_c with its odd ones because of the antisymmetry, e.g., $Pe\rightarrow -Pe$ with $x\rightarrow -x$. The solution of O(1) through substitution of Eqs. (10) into (9) has the same results as Eqs. (7) for the case of no throughflow, i.e., $R_{c,0}=4\pi^2$ with $a_{c,0}=\pi$. Using equations for O(Pe), O(Pe^2) and O(Pe^3), $\omega_{c,1}$, v_p, $R_{c,2}$ and $a_{c,2}$ are obtained:

$$\omega_{c,1}=\pi,\ v_p=Pe,\ R_{c,2}=a_{c,2}=0, \tag{11a-c}$$

where $v_p=\omega/a$. The phase speed v_p is the same as the dimensionless main flow velocity Pe. The above instability conditions lead to Eqs. (7) for Pe<<1 (see Eqs. (10)). With throughflow traveling transverse rolls can set in.

3. Weakly Nonlinear Analysis

The evolution of cellular structure slightly over the critical Darcy-Rayleigh number $R_{c,0}$ has been investigated intensively. For the present system Dufour and Neel [13] derived the GLE using the multiple scale analysis. However, some coefficients in their equation are not in accordance with those derived from linear theory, which produces the unreasonable stability criteria. Therefore, for the present system the GLE is re-derived and its instability is examined.

With the basic state of u_0=Pe, w_0=0 and θ_0=1−z, the perturbed quantities Ψ and Θ to represent two-dimensional transverse rolls are introduced:

$$\psi(x,z,\tau)=\Psi,\ \theta(x,z,\tau)=1-z+\Theta, \tag{12a,b}$$

where ψ denotes the dimensionless stream function. The nonlinear perturbed equations are derived from substitution of Eqs. (12) into (2)-(4):

$$\nabla_2^2\Psi=R\frac{\partial\Theta}{\partial x}, \tag{13a}$$

$$\frac{\partial\Theta}{\partial\tau}=-Pe\frac{\partial\Theta}{\partial x}+\frac{\partial\Psi}{\partial x}+\frac{\partial\Psi}{\partial z}\frac{\partial\Theta}{\partial x}-\frac{\partial\Psi}{\partial x}\frac{\partial\Theta}{\partial z}+\nabla_2^2\Theta, \tag{13b}$$

where $\nabla_2^2=\partial^2/\partial z^2+\partial^2/\partial x^2$. The boundary conditions are given as

$$\Psi=\Theta=0 \quad \text{at} \quad z=0 \quad \text{and} \quad z=1. \tag{13c}$$

In order to obtain the solution of Eqs. (13), Ψ and Θ are expanded

near the critical condition, $R \cong R_c$:

$$\begin{pmatrix} \Psi \\ \Theta \end{pmatrix} = \mu \begin{pmatrix} \Psi_1 \\ \Theta_1 \end{pmatrix} + \mu^2 \begin{pmatrix} \Psi_2 \\ \Theta_2 \end{pmatrix} + \mu^3 \begin{pmatrix} \Psi_3 \\ \Theta_3 \end{pmatrix} + \cdots, \tag{14}$$

where $\mu(=R/R_c-1)$ represents the degree of deviation from the critical condition in case of $U_0 \neq 0$. Here, R_c represents the critical Darcy-Rayleigh number in the presence of throughflow. Now, R and Pe are expanded as $R-R_c=\sum_{n=1}^{\infty}\mu^n R_{c,n}$ and $Pe=\sum_{n=0}^{\infty}\mu^n Pe_n$. Also, the slow multiple scales are introduced to both the space $X_1=\mu x$; $X_2=\mu^2 x$; …, and the time $T_1=\mu\tau$, $T_2=\mu^2\tau$, … [14].

Based on the above relations, the perturbed equations of $O(\mu)$ are produced as

$$\nabla_2^2 \Psi_1 = R_c \frac{\partial \Theta_1}{\partial x}, \tag{15a}$$

$$\frac{\partial \Theta_1}{\partial \tau} = \nabla_2^2 \Theta_1 - Pe_0 \frac{\partial \Theta_1}{\partial x} + \frac{\partial \Psi_1}{\partial x}. \tag{15b}$$

Using the frame of $\xi = x - Pe_0\tau$ at $a_c=\pi$, the above equations produce the same solutions with those of Prats [3]:

$$\Psi_1 = -\frac{i}{\pi}[A_1 \exp\{i(a_c x - \omega_c \tau)\} - c.c.]\sin(\pi z), \tag{16a}$$

$$\Theta_1 = -\frac{1}{2\pi^2}[A_1 \exp\{i(a_c x - \omega_c \tau)\} + c.c.]\sin(\pi z), \tag{16b}$$

where A_1 denotes the amplitude. In case of $Pe_0 \to 0$, with $\partial\Theta_1/\partial T_1 + Pe_0 \partial\Theta_1/\partial X_1 = 0$, the $O(\mu^2)$ solutions are obtained as

$$\Psi_2 = 0, \tag{17a}$$

$$\Theta_2 = -\frac{1}{4\pi^3} A_1 \overline{A_1} \sin(2\pi z), \tag{17b}$$

where $\overline{A_1}$ denotes the amplitude of the complex conjugate solution of the $O(\mu)$ equations.

Applying $\partial\Theta_2/\partial T_1 + Pe_0 \partial\Theta_2/\partial X_1 = 0$ to the $O(\mu^3)$ equations, their inhomogeneous parts have to be orthogonal to the adjoint solution of the $O(\mu)$ equations, that is called the solvability condition: $\langle N_1|\Psi^*\rangle + \langle N_2|\Theta^*\rangle = 0$. The bracket denotes integration over the whole domain, and the symbols of N_1 and N_2 represent the inhomogeneous parts of perturbed motion and energy equations in $O(\mu^3)$, respectively. The adjoint solutions Ψ^* and Θ^* are represented by

$$\begin{pmatrix} \Psi^* \\ \Theta^* \end{pmatrix} = \begin{pmatrix} i/\pi \\ 1/(2\pi^2)R_c \end{pmatrix} \exp[-i(a_c x - \omega_c \tau)]\sin(\pi z). \tag{18}$$

Using the above condition and the scale relations and $A(x, \tau) = \mu A_1(\mu x, \mu\tau)$, the amplitude of the $O(\mu^3)$ equations is derived newly here:

$$\frac{1}{2\pi^2}\left(\frac{\partial}{\partial \tau} + Pe\frac{\partial}{\partial x}\right)A = \left[\frac{I_-}{I_+}\mu + \frac{1}{2\pi^2}\left(1 + \frac{4\pi^2 I_-}{R_c I_+}\right)\frac{\partial^2}{\partial x^2} - \frac{1}{4\pi^2}A\overline{A}\right]A. \tag{19a}$$

The coefficients are obtained from integration:

$$I_+ = \frac{R_c}{8\pi^4}\int_0^{2a_c/\omega_c}\int_0^2 [1 + \exp\{-2i(a_c x - \omega_c \tau)\}]dx d\tau, \tag{19b}$$

$$I_- = \frac{R_c}{8\pi^4}\int_0^{2a_c/\omega_c}\int_0^2 [1 - \exp\{-2i(a_c x - \omega_c \tau)\}]dx d\tau, \tag{19c}$$

The integration is done for a cross sectional area of one vortex pair over x=0-2 during one period ($\tau = 2a_c/\omega_c$). It is noted that $I_-/I_+ = 1$ with $a_c = \pi$.

Now, Eqs. (19) are compared with the general form of complex GLE,

$$\tau_0\left(\frac{\partial}{\partial \tau} + v_g\frac{\partial}{\partial x}\right)A = \left[\mu(1+ic_0) + \xi_0^2(1+ic_1)\frac{\partial^2}{\partial x^2} - \tilde{\lambda}(1+ic_2)|A|^2\right]A. \tag{20}$$

The real coefficients τ_0 and ξ_0^2, and the imaginary ones c_0 and c_1 can be obtained from the dispersion relation around the critical wavenumber a_c. The coefficient v_g is the group velocity ($=\partial\omega/\partial a|_c$). By comparing Eqs. (19) with (20) the real coefficients in (20) are obtained easily with $a_c = \omega_c/Pe = \pi$ and $R_c = 4\pi^2$:

$$\tau_0 = \frac{1}{2\pi^2},\ v_g = Pe,\ \xi_0^2 = \frac{1}{\pi^2},\ \tilde{\lambda} = \frac{1}{4\pi^2}, \tag{21a-d}$$

where τ_0 and ξ_0^2 from Eqs. (19) are identical with those from linear theory through the relations of $\tau_0^{-1} = R(\partial\sigma_r/\partial R)|_c$ and $\xi_0^2 = (\partial^2 R/\partial a^2)/(2R)|_c$. It is noted that $v_g = v_p = Pe$ in the present system. The relation of $\tau_0 = \xi_0^2 = 1/(4\pi)$ by Dufour and Neel [13] does not satisfy the above relations. It is known that from Eqs. (19) the imaginary coefficients of the imaginary part $c_0(=-R\tau_0(\partial\omega/\partial R)|_c)$, $c_1(=\tau_0/(2\xi_0^2)(\partial^2\omega/\partial a^2)|_c)$ and c_2 in Eq. (20) are all zero (see Eqs. (7) and (11)).

According to the conventional stability criterion [14,15] the critical condition of the overstability appears at $\mu = \mu_c^{conv}$, where $\sigma_r = 0$ but $\sigma_i \neq 0$ in Eq. (5). The system is absolutely unstable when $\mu > \mu_c^{conv}$ because $\sigma_r > 0$. When $0 < \mu < \mu_c^{conv}$ the system is convectively unstable because $\sigma_r < 0$ but $\sigma_i \neq 0$. In the latter regime a local perturbation in form of transverse rolls cannot propagate upstream since $v_p = v_g$ and will finally die out. But other modes of instabilities, e.g., longitudinal rolls, can set in. For $\mu < 0$ the system is absolutely stable and all the perturbed quantities will disappear everywhere with time. The μ_c^{conv}-value is obtained by replacing A in Eq. (19a) with $\exp[i(a_c x - \omega_c \tau)]$ and the condition of $\sigma_r = 0$ but $\sigma_i \neq 0$:

$$\mu_c^{conv} = \frac{\tau_0^2 v_g^2}{4\xi_0^2}, \tag{22}$$

which is the same as the previous ones [14,15] with $c_1 = 0$. Considering that the Darcy law is valid for $Da(=K/H^2) < 10^{-4}$, the present criterion seems to be acceptable to the slow flow regime. The region of the oscillating behavior which was observed by Combarnous and Bia [4] is embedded in the absolute unstable region: $\mu > \mu_c^{conv}$.

4. Numerical Simulation

It is the 3-dimensional phenomenon that with an increase in flow rate the flow-change from the oscillating transverse roll to the stationary longitudinal roll occurs. Therefore, the governing Eqs. (2)-(4) are solved numerically in 3-dimensional Cartesian coordinates. The finite difference scheme considering a control volume is employed. The general staggered grid is used during the mesh along the x-, y- and z-direction consisting of 80×20×10. In addition, for fast convergence to reduce an error between the analytic solution and the numerical one in conduction state during early time step, a vertical non-uniform fine mesh is adopted. To solve non-linearly coupled velocity and pressure equations the well-known SIMPLE method [16] is used. For time-dependent marching the implicit scheme is applied. The typical benchmark result using the present numerical

scheme is compared with the well known one of Blankenbach et al. [17] for pure fluid layer and has good agreement with them.

There are two kinds of aspect ratios, Γ_x(=L/H) and Γ_y(=W/H), where L and W are the streamwise length and the spanwise width, respectively. It is an important question to specify the suitable computational domain size. Here we selected Γ_x=10 and Γ_y=2. For an observation of downward traveling transverse rolls, it is reasonable to choose the domain length of $\Gamma_x > \Gamma_y$, because the initiate rolls are aligned perpendicular to the long wall to reduce the dissipation energy. Considering the purpose of this study to observe the phase transition phenomena near the critical condition, i.e. R=R_c, the wave number a of steady longitudinal vortices almost become π. By means of the wave number the spanwise width, i.e., the wave length λ(=2πH/a), should be 2.

Under neglecting the thermal dispersion effect, the present simulation is valid for Darcy number Da<10^{-4} [18]. For an initial condition, the periodic perturbed quantities are imposed at inlet boundary, similar to Chen and Lavine [19]. However, we selected the amplitude of an initial fluctuation as $\theta_{1,max}=10^{-3}$, which selection is well described in the work of Choi et al. [20]. The boundary conditions are given as

$$u=v=w=\theta-1=0 \text{ at } z=0, \tag{23a}$$

$$u=v=w=\theta=0 \text{ at } z=1, \tag{23b}$$

$$u=v=\frac{\partial w}{\partial y}=\frac{\partial \theta}{\partial y}=0 \text{ at } y=0 \text{ and } y=1. \tag{23c}$$

Here u, v and w represent the streamwise, the spanwise and the vertical velocities, respectively. The upper and lower boundary conditions are the same as those of the previous section. For the assumption of the horizontally infinite boundary conditions, the vertical shear free and the adiabatic conditions are applied at the side walls, as shown in Fig. 1.

RESULTS AND DISCUSSION

1. Absolute and Convective Instabilities

It is well known to anyone who observes the Poiseuille flow heated from below that the convective rolls travel along with primary flow [21]. For a fluid saturated porous medium heated from below under the existence of primary basic flow, Prats [3] tested the possibility of a time-dependent oscillating wave, and Combarnous and Bia [4] first reported on the experimental observation of wavy motion as well as the critical condition of appearance of the steady standing wave.

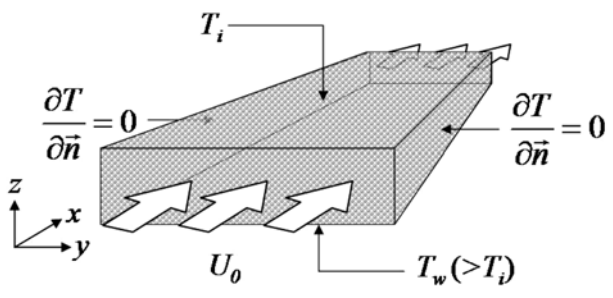

Fig. 1. Sketch of laminar forced convection system considered in the present study.

Under linear theory, the infinitesimal perturbed disturbances grow exponentially or disappear in unstable or stable states, respectively (see Eq. (5)). However, it is difficult to determine the stability of small fluctuations in nonlinear equations. Choi et al. [20] proposed temporal growth rate of velocity and temperature fields in the Rayleigh-Bénard convection system. In their study, the growth rate for fluctuation fields is defined under the concept of energy identity, $E_1\left(=1/2\int_V (\mathbf{u}'^2+bPrR\theta'^2)dV\right)$ in the energy method suggested by Joseph [22]. Here Pr(=ν/α) and V denote Prandtl number and volume of system in their study. Also b means coupling parameter between kinetic and thermal energies. According to their procedure, the temporal growth rate r_1 of fluctuations is defined as

$$r_1=\frac{1}{E_1^{1/2}}\frac{dE_1^{1/2}}{d\tau}. \tag{24}$$

Here, the concept of r_1 is the same as the real part of σ in Eq. (5). For the Darcy-Boussinesq system, the energy identity is already derived by Gill [23]. According to his study, the energy identity based on Darcy equation is only constituted with thermal disturbance, θ_1. Hence, the energy identity E_1 in Eq. (24) is only a function of θ_1. In the present system, the driving forces are buoyancy and inertial, R and Pe. When a fluid flows through a porous media heated from below, the growth rate of disturbance for the steady laminar convection depends only on the primary direction, i.e., longitudinal rolls or helicoidal vortices [10]. Therefore, the fluctuation grows with time τ as well as the primary flow direction x. It is reasonable that the local growth rate for θ_1 is defined as

$$r_1(\tau,x)=\frac{1}{E_1^{1/2}}\frac{dE_1^{1/2}}{dx}. \tag{25}$$

For the time-dependent oscillating region, $\mu>\mu_c^{conv}$ with $\sigma_r>0$ and $\sigma_i\neq 0$, fluctuations evolve through the overall domain because the system is absolute unstable. To observe a continuous down traveling wave, we selected the following two parameters, R=43 and Pe=0.4. In Fig. 2, the isothermal surfaces of the well-formed transverse rolls are featured with finite time step. As expected, the rolls are aligned to a shorter wall and flow to downstream. It is noted that any perturbations do not decay in this region. In the figure the arrows denote the traveling same rolls. It is the same result as of Dufour

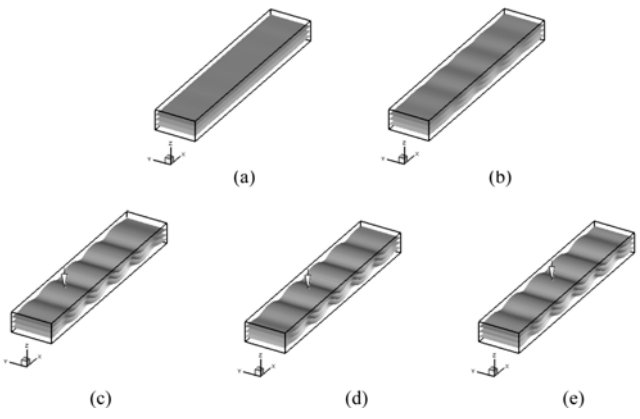

Fig. 2. Traveling waves with time for R=43 and Pe=0.4: (a) τ=0 (b) τ=3 (c) τ=5 (d) τ=7 (e) τ=9.

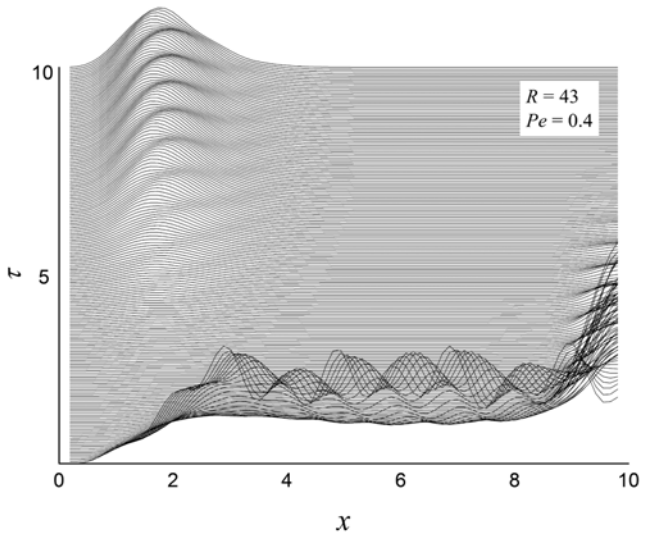

Fig. 3. Spatiotemporal diagram of local growth rate r_1 for R=43 and Pe=0.4.

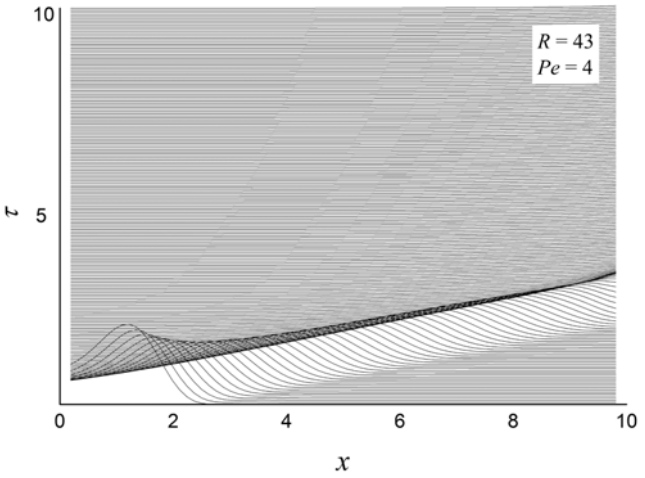

Fig. 5. Spatiotemporal diagram of local growth rate r_1 for R=43 and Pe=3.

and Neel [13] except for μ_c^{conv}-value derived from the weakly nonlinear stability analysis. With the definition of Eq. (25), the growth rate of local disturbances spreads through the whole space-time domain, as shown in Fig. 3. Its behavior is the same as with the schematic diagram for absolute instabilities sketched by Huerre [24] (Fig. 1 in his study).

Similarly, for $0<\mu<\mu_c^{conv}$ with $\sigma_r<0$ but $\sigma_i\neq 0$, Huerre [24] showed the breaking out of convective nature of primary instabilities with using the Newell-Whitehead-Segel evolution model [25,26]. In the present system, it means that the disturbances travel downstream with an increase in inertial force, and disappear at a certain position. With a slow increase in Pe-value, we observed the convective motion for a given R-value. At Pe=3 for the finite domain, the traveling rolls finally disappeared at the outlet after a certain time, as shown in Fig. 4. As explained by Huerre [24], the input disturbances travel toward downstream as that of absolute unstable region, and finally disappear near the outlet. Here, the position of the ripple of the isothermal surface marked by the arrows is in accordance with the local maximum of growth rate, as shown in Fig. 5. The corresponding spatiotemporal behavior in Fig. 5 is exactly matched with the conceptual sketch of Huerre [24] on the convective instability. The locally asymptotic stability is applicable to the present finite domain. However, the stability condition for the global domain is inconsistent with that of a local one. Assuming that the domain is extended to the infinite, the disturbances or the transverse rolls flow to a certain space-time domain (see Fig. 5). Therefore, the global convective instabilities are also applicable to this case.

To simulate the flow change from transverse wave type rolls (T-mode) to longitudinal vortex type ones (L-mode), the Pe-value is gradually increased at R=100. The time-dependent oscillating transverse rolls are traveling toward downstream and disappear, and then the stationary longitudinal rolls are observed near downstream, as shown in Fig. 6. This phenomenon is the same as that of Coma-

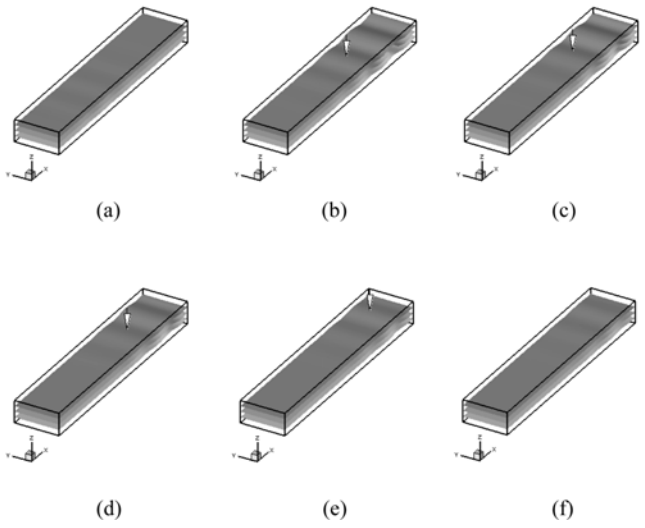

Fig. 4. Traveling waves with time for R=43 and Pe=3: (a) τ=0 (b) τ=3 (c) τ=6 (d) τ=9 (e) τ=12 (f) τ=15.

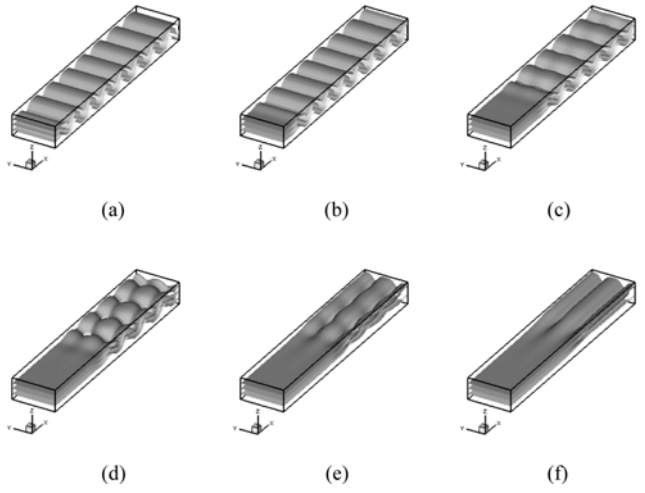

Fig. 6. Phase change with an increase of Pe-value for R=100: (a) Pe=7 (b) Pe=15 (c) Pe=21 (d) Pe=22 (e) Pe=23 (f) Pe=24.

barnous and Bia [4]. However, their fixed value, Pe≅7.6, shows the phase transition was not observable in this system. The detailed stability condition related to this phase transition is discussed in the next section.

2. Stability Condition

On the phase transition of mixed convection in porous media, thorough experiments are conducted by Combarnous [4,11,12]. Especially, he examined broadly the characteristic effects, i.e., the inertia effect by Forchheimer term in hydrodynamic relation or the effect of local thermal non-equilibrium between solid and fluid. However, in the present study, our interest sets a limit to the laminar Darcy regime upon the condition of local thermal equilibrium. Therefore, the present analysis compares with a few parts of his experimental data, e.g., 3 mm and 4mm of glass bead and water system (series 11 and 6 in his thesis [11]). The dimensionless parameters characterizing these series are $Da=2.5\times10^{-6}$ and Pe=7.7 for 3 mm glass bead and $Da=4.0\times10^{-6}$ and Pe=6.9 for 4 mm one, respectively. These values correspond to the characteristics of the Darcy region. The open circle (○) and triangle (△) denote the appearance of T-mode rolls and L-mode ones, respectively, as shown in Fig. 7. The dotted line from linear stability analysis marked $R=4\pi^2$ as the lower boundary of instability, i.e., no buoyancy-driven convective motion below its value. The weakly nonlinear analyses represented the solid line for the present study and the dashed line for that of Dufour and Neel [13]. Here, the closed circle (●) and triangle (▲) denote the T-mode and L-mode from the present numerical simulation, respectively. Both the solid line and dashed line are close to the results of numerical simulation (●) near $R=4\pi^2$. However, as an increase with Pe-value, the two analyses are separated. The solid line from the present study is more close to the experiment results than the dashed line from Dufour and Neel [13]. The difference between the two analyses seems to be due to the discrepancy between two criteria, as explained in section 3 of the theoretical analysis part. In the upper regime of the solid line ($R>R_c^{conv}$) a flow becomes absolutely unstable; on the other side a flow comes to be convectively unstable below R_c^{conv}-value. It is noted that in both cases of theoretical and experimental approaches the phase transition from T-mode to L-one did not appear just below R_c^{conv}-value, because the domain of considered system is confined, i.e., the aspect ratio of the experiment is 6.9 and that of the present study 5, respectively. If the aspect ratio becomes infinite, this discrepancy will disappear.

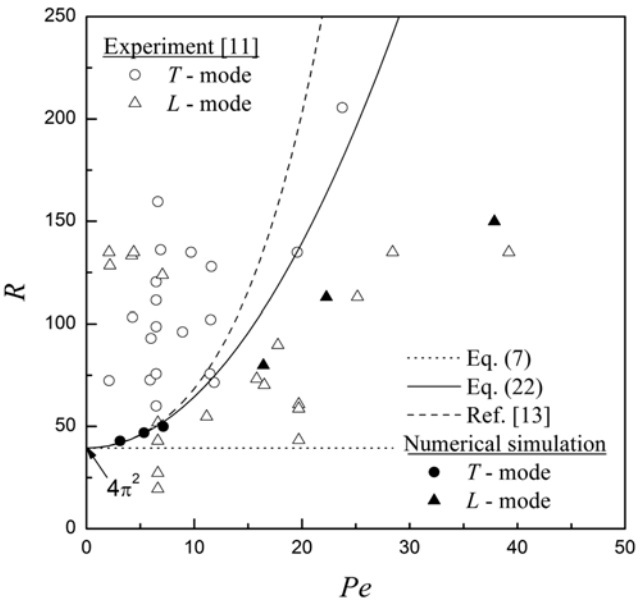

Fig. 7. Instability map on absolute and convective instabilities for laminar forced convection in porous media.

Taking all of the above results into consideration, for the horizontal porous layer heated from below with throughflow, the system becomes absolutely unstable for $R>R_c^{conv}$ and comes to be convectively unstable for $R_{c,0}<R<R_c^{conv}$. Also, the buoyancy-driven convection disappears for $R<R_{c,0}$.

CONCLUSION

The stability criteria on the mixed convection of porous media were obtained from linear stability analysis, weakly nonlinear analysis and direct numerical simulation. These results compared with available theoretical and experimental results. For small Pe-value, the stability condition is the same as that of the Horton-Rogers-Lapwood criterion, $R_{c,0}=4\pi^2$. In addition, a reasonable stability criterion (μ_c^{conv}) between absolute and convective instabilities was derived, and had good agreement with the experiment data. We expect that the present analysis gives a definite key to slightly forced convection flow through porous media.

ACKNOWLEDGMENT

T. J. Chung acknowledges that his scientific ground is hardened by the passionate guidance of Professor C. K. Choi, whom he thanks for the advice and the teaching.

REFERENCES

1. C. W. Horton and F. T. Rogers, *J. Appl. Phys.*, **16**, 367 (1945).
2. E. R. Lapwood, *Proc. Camb. Phil. Soc.*, **44**, 518 (1948).
3. M. Prats, *J. Geophys. Research*, **71**, 4835 (1966).
4. M. A. Combarnous and P. Bia, *Soc. Pet. Eng. J.*, **251**, 399 (1971).
5. C. T. Hsu and P. Cheng, *Int. J. Heat Mass Transfer*, **23**, 798 (1980).
6. M. C. Kim, J. S. Baik, I. G. Hwang, D.-Y. Yoon and C. K. Choi, *Chem. Eng. Sci.*, **54**, 619 (1999).
7. J. H. Park, T. J. Chung, C. K. Choi and M. C. Kim, *AIChE J.*, **52**, 2677 (2006).
8. C. K. Choi, T. J. Chung and M. C. Kim, *Int. J. Heat Mass Transfer*, **47**, 2629 (2004).
9. D. H. Lee, D.-Y. Yoon and C. K. Choi, *Int. J. Heat Mass Transfer*, **43**, 2895 (2000).
10. T. J. Chung, J. H. Park, C. K. Choi and D.-Y. Yoon, *Int. J. Heat Mass Transfer*, **45**, 3061 (2002).
11. M. Combarnous, *Convection naturelle et convection mixte en milieu poreux*, Ph.D. thesis, Faculté des sciences de l'univ. de Paris (1970).
12. A. Delache, M. N. Ouarzazi and M. Combarnous, *Int. J. Heat Mass Transfer*, **50**, 1485 (2007).
13. F. Dufour and M.-C. Neel, *Phys. Fluids*, **10**, 2198 (1998).
14. H. W. Müller, M. Lücke and M. Kamps, *Phys. Rev. A*, **45**, 3714 (1992).

15 A. Recktenwald, M. Lücke and H. W. Müller, *Phys. Rev. E*, **48**, 4444 (1993).
16. S. V. Patankar, *Numerical heat transfer and fluid flow*, Taylor and Francis (1980).
17. B. Blankenbach, F. Busse, U. Christensen, L. Cserepes, D. Gunkel, U. Hansen, H. Harder, G. Jarvis, M. Koch, G. Marquart, D. Moore, P. Olson, H. Schmeling and T. Schanubelt, *Geophys. J. Int.*, **98**, 23 (1989).
18. K. L. Walker and G. M. Homsy, *J. Fluid Mech.*, **87**, 449 (1978).
19. S. S. Chen and A. S. Lavine, *Int. J. Heat Mass Transfer*, **39**, 1 (1996).
20. C. K. Choi, J. H. Park, H. K. Park, H. J. Cho, T. J. Chung and M. C. Kim, *Int. J. Thermal Sci.*, **43**, 817 (2004).
21. M. T. Ouazzani, J. P. Caltagirone, G. Meyer and A. Mojtabi, *Int. J. Heat Mass Transfer*, **32**, 261 (1989).
22. D. D. Joseph, *Stability of fluid motions I and II*, Springer-Verlag, New York (1976).
23. A. E. Gill, *J. Fluid Mech*., **35**, 545 (1969).
24. P. Huerre, *Propagation in system far from equilibrium*, edited by J. E. Wesfreid, H. R. Brand, P. Manneville, G. Albinet and N. Boccara, 340 (1988).
25. A. C. Newell and J. A. Whitehead, *J. Fluid Mech.*, **38**, 279 (1969).
26. L. Segel, *J. Fluid Mech.*, **38**, 203 (1969).